photochem

MDPI

Article

Electronic Absorption, Emission, and Two-Photon Absorption Properties of Some Extended 2,4,6-Triphenyl-1,3,5-Triazines

Alison G. Barnes [1], Nicolas Richy [1], Anissa Amar [2,3], Mireille Blanchard-Desce [4], Abdou Boucekkine [1,*], Olivier Mongin [1] and Frédéric Paul [1,*]

[1] Univ. Rennes, CNRS, ISCR (Institut des Sciences Chimiques de Rennes)-UMR 6226, F-35000 Rennes, France; sidereus.nuncius.au@gmail.com (A.G.B.); nicolas.richy@univ-rennes1.fr (N.R.); olivier.mongin@univ-rennes1.fr (O.M.)
[2] Laboratoire de Physique et Chimie Quantiques, Faculté des Sciences, Université Mouloud Mammeri de Tizi-Ouzou, Tizi-Ouzou 15000, Algeria; anissa.amar@ummto.dz
[3] Faculté de Chimie, Université des Sciences et de la Technologie Houari-Boumediene, Bab-Ezzouar 16111, Algeria
[4] Univ. Bordeaux, CNRS, ISM (Institut des Sciences Moléculaires)-UMR 5255, F-33400 Talence, France; mireille.blanchard-desce@u-bordeaux.fr
* Correspondence: abdou.boucekkine@univ-rennes1.fr (A.B.); frederic.paul@univ-rennes1.fr (F.P.); Tel.: +33-02-23-23-59-62 (F.P.)

Abstract: We report herein the linear optical properties of some extended 2,4,6-triphenyl-s-triazines of formula 2,4,6-[(1,4-C_6H_4)C≡C(4-C_6H_4X)]$_3$-1,3,5-($C_3H_3N_3$) (**3-X**; X = NO_2, CN, OMe, NMe_2, NPh_2) and related analogues **4** and **7-X** (X = H, NPh_2), before briefly discussing their two-photon absorption (2PA) cross-sections. Their 2PA performance is discussed in relation to 2PA values previously measured for closely related octupoles such as *N*,*N*′,*N*″-triphenylisocyanurates (**1-X**, **5**, and **6-X**) or 1,3,5-triphenylbenzenes (**2-X**). While s-triazines are usually much better two-photon absorbers in the near-IR range than these molecules, especially when functionalised by electron-releasing substituents at their periphery, they present a decreased transparency window in the visible range due to their red-shifted first 1PA peak, in particular when compared with corresponding isocyanurates analogues. In contrast, due to their significantly larger two-photon brilliancy, 2,4,6-triphenyl-s-triazines appear more promising than the latter for two-photon fluorescence bio-imaging purposes. Rationalisation of these unexpected outcomes is proposed based on DFT calculations.

Keywords: 2,4,6-triaryl-s-triazines; octupoles; two-photon absorption; DFT calculations; fluorescence; linear optics

Citation: Barnes, A.G.; Richy, N.; Amar, A.; Blanchard-Desce, M.; Boucekkine, A.; Mongin, O.; Paul, F. Electronic Absorption, Emission, and Two-Photon Absorption Properties of Some Extended 2,4,6-Triphenyl-1,3,5-Triazines. *Photochem* **2022**, *2*, 326–344. https://doi.org/10.3390/photochem2020023

Academic Editor: Marcelo I. Guzman

Received: 28 March 2022
Accepted: 12 May 2022
Published: 19 May 2022

1. Introduction

Planar molecules featuring trigonal symmetry have attracted sustained attention for their second-order nonlinear optical (NLO) properties since the late eighties [1–4]. Initially aroused by the quest for molecules with large second-order NLO properties, these so-called "octupolar" molecules were likely to exhibit sizeable hyperpolarizabilities due to their peculiar symmetry, in reason of the existence of off-diagonal tensorial elements in the electronic coupling matrix between peripheral branches [2]. It was subsequently shown that this symmetry can also be potentially beneficial to third-order NLO properties such as two-photon absorption (2PA). Given the very appealing societal prospects for dyes presenting large 2PA cross-sections [5–8], in particular regarding fluorescence bio-imaging when the dye also fluoresces [6,9], we have started exploring the 2PA properties of various families of molecules, such as extended 1,3,5-triaryltriazinane-2,4,6-triones (**1-X**; Scheme 1) [10,11] or 1,3,5-triphenylbenzene (**2-X**) [12]. Both **1-X** (also known as *N*,*N*′,*N*″-triphenylisocyanurates [13]) and **2-X** derivatives proved to be good two-photon absorbers, especially when functionalised by electron-releasing groups at their periphery [11,12]. Actually, in line with these findings as well as with independent reports [14], we observed that

the cross-section of the first 2PA peak for these derivatives increased with the polarisation of the peripheral arms, typically when strongly electron-releasing X substituents were present (X = OMe, NMe_2, NPh_2). However, we also observed that upon progressing from the isocyanurate core (**1-X**) to the slightly less electron-deficient 1,3,5-phenylene core (**2-X**), a slight decrease in the 2PA cross-section occurred for the latter derivatives but only for the most electron-releasing substituents. This suggested that the polarisation induced by the former core was slightly more favourable to 2PA than that induced by the second.

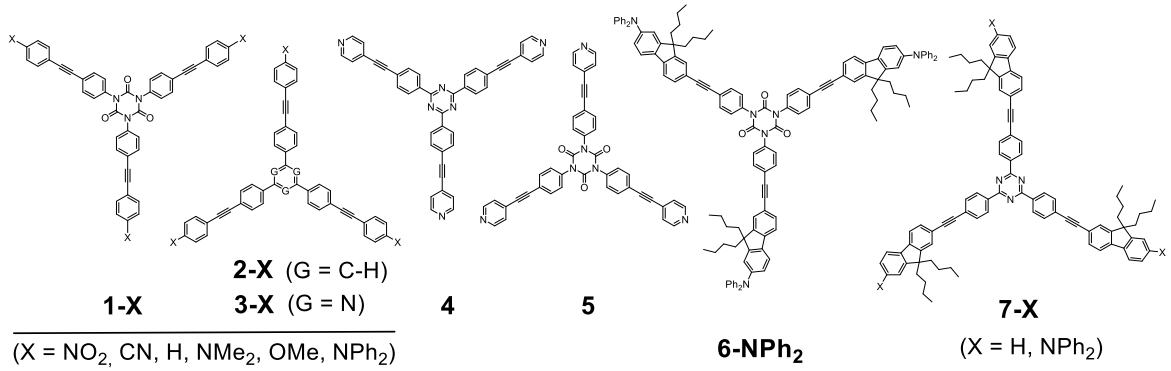

Scheme 1. Molecular structures of known and targeted compounds.

In this respect, surmising that the 1,3,5-triazine core was more electron-attracting than the isocyanurate one, it was now interesting to study the 2PA properties and the fluorescence of related 1,3,5-triazine analogues of **1-X** such as **3-X** (X = NO_2, CN, OMe, NMe_2, and NPh_2). Thus far, emissive triphenyl-s-triazine derivatives and related extended analogues have mainly raised interest in the field of OLEDs or closely related fields [15–18]; however, very few studies were actually focused on the NLO properties of such derivatives. While related derivatives such as extended trialkynyl-s-triazines [19], trialkenyl-s-triazines [20,21], or tris(2-thienyl)-s-triazines [22–25] have given rise to some 2PA investigations, to the best of our knowledge, only one recent theoretical paper deals specifically with the second-order NLO properties of molecules such as **3-X** [26], and only one other single paper addresses the 2PA properties of an s-triazine derivative closely related to **7-H** [27]. Thus, regarding extended triphenyl-s-triazines, essentially styryl-type analogues of **3-X** have been investigated so far for their 2PA properties [28–30]. A general experimental and theoretical study focused on the 2PA properties of octupolar compounds such as **3-X** and **7-X** would therefore be timely. Furthermore, anticipating the well-known propensity of nitro substituents to poison fluorescence in **3-NO_2**, we also targeted a derivative such as **4**, which similar to **3-CN**, constitutes another example of a compound featuring electron-withdrawing arms [31]. The optical properties of this new triazine derivative might then be compared with those of its known isocyanurate analogue (**5**) [32]. Finally, given that the extended 4-fluorenyl derivative **6-NPh_2** exhibits the most promising optical properties for bio-imaging purposes among all triarylisocyanurates studied so far [33], the study of triazine analogues such as **7-X** (X = H, NPh_2) was also required. Accordingly, in the following we will first start with the synthesis of the targeted molecules (**3-X**, **4,** and **7-X**) and study the 2PA properties of their emissive representatives via two-photon excited fluorescence (TPEF). Their optical properties of interest will then be discussed with the help of density functional theory (DFT) and time-dependent DFT (TD-DFT) calculations.

2. Results

2.1. Synthesis and Characterisation

The desired **3-X**, **4,** and **7-X** derivatives are structurally close to known s-triazine derivatives [15–17,27,34–40]. The **3-X** series corresponds to the simplest derivatives in which the 1,3,5-triphenyl-s-triazine core has been extended with a phenyl–alkynyl linker and terminated with X-groups of varying electron-donor/acceptor power. The second

series (**7-X**) involves replacing the second phenyl unit with a 2-fluorenyl unit, which is luminescent in its own right. All these derivatives were obtained via Sonogashira coupling reactions (Scheme 2) from the known bromo [17,41–43] or iodo [43] precursors **8-Y**, after reaction with the corresponding aromatic alkynes. Most of these products required chromatographic purification. The use of **8-I** instead of **8-Br** allows generally using smother reaction conditions or leads to higher yields of isolated coupling products under similar conditions. Several **3-X** derivatives have already been reported, such as **3-CN** [17], **3-OMe** [15], and **3-NPh$_2$** [18]. All other compounds were new and were fully characterised by usual techniques. However, synthesis of the nitro derivative **3-NO$_2$**, due solubility issues, was very problematic by such an approach and had to be attempted from the known triyne **8-C≡CH** [16,18], itself obtained in two steps from **8-Br**. Regarding IR-characterization, the in-plane ring stretches of the s-triazine ring resemble those of the phenyl ring and are not so characteristic of triphenyl-s-triazines [44], except perhaps for the fully symmetric stretch (only Raman-active), around 990 cm^{-1} [45,46].

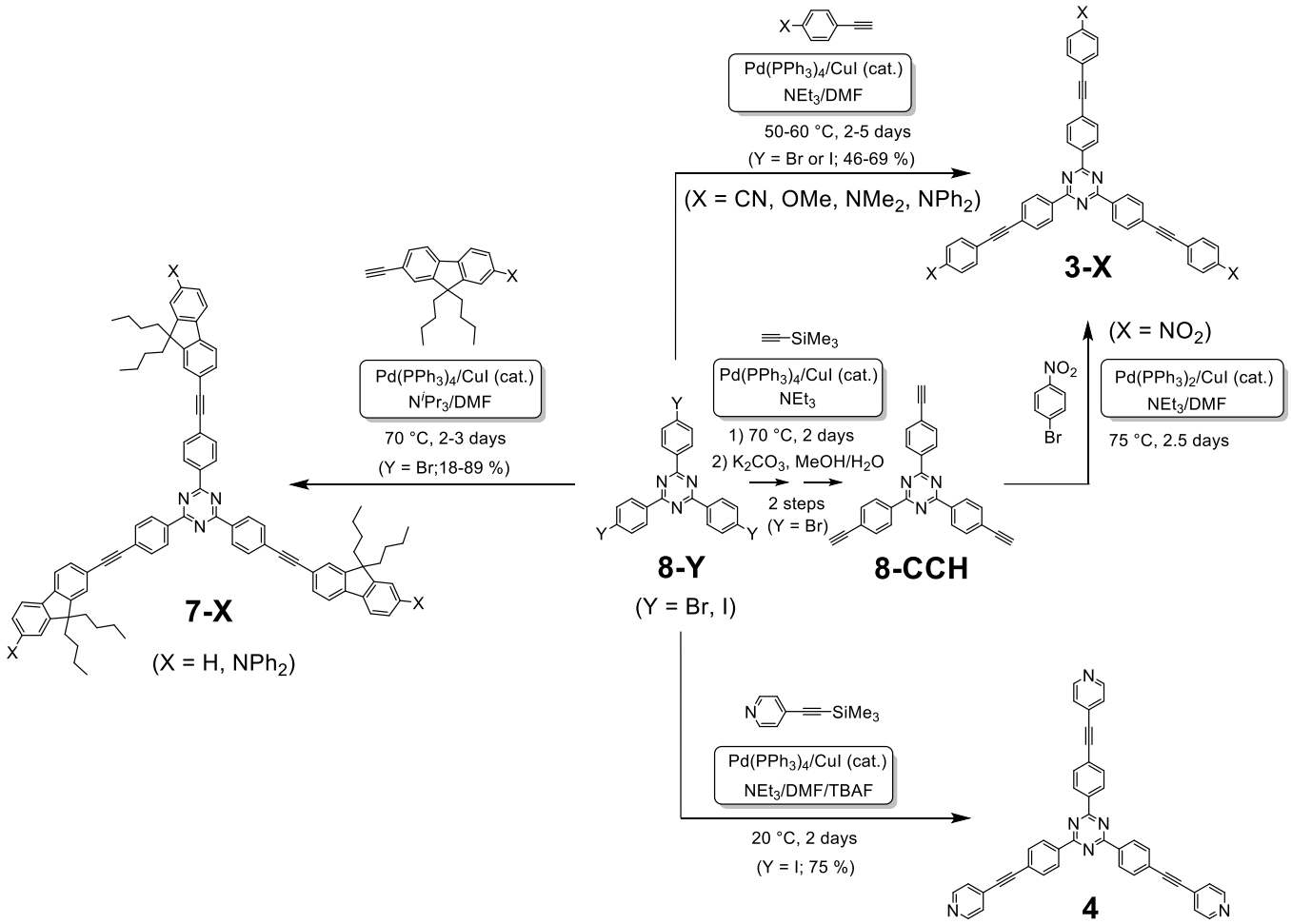

Scheme 2. Synthesis of **3-X**, **4**, and **7-X** derivatives.

2.2. One- and Two-Photon Absorption and Emission Studies

The UV–Vis absorption spectra of the various triazine derivatives were recorded. Except for **3-CN** and **4**, most of the extended compounds (**3-X** and **7-X**) absorbed significantly in the visible range and were strongly coloured (deep yellow in solution), with a lowest-energy absorption entailing significantly above 400 nm (Table 1). Upon progressing from **4** to **3-NPh$_2$** (corresponding to an increase in the electron-releasing nature of the *para*-substituents), a bathochromic shift of the first absorption was clearly observed (Figure 1). A similar trend could also be observed when progressing from **4** to **3-NO$_2$**.

For a given substituent in the **3-X** series, the intensity of the lowest-energy absorption was comparable with that of **1-X** or **2-X** analogues. A higher-energy absorption (at ca. 270–325 nm) was also observed for all these derivatives. The latter became of comparable intensity to the one at the lowest energy for the compounds with the most electron-releasing substituents. Except for **3-NO_2**, **3-CN**, and **4**, all extended derivatives were significantly luminescent in CH_2Cl_2 solutions (Table 1). Luminescence was maximal (Φ_F = 0.80) for the fluorenyl derivative **7-H**. The fluorescence of **3-X** and **4** was comparable to that of their isocyanurate analogues (**1-X** and **5**) but was overall slightly lower than that of their known 1,3,5-triphenylbenzene analogues (**2-X**). In contrast, the fluorescence quantum yield of **7-NPh_2** was roughly one-fourth of that previously found for **6-NPh_2** (Φ_F = 0.78). In all cases, mirror-symmetry relationships between the first absorption and emission bands and energetic differences between their maxima (see ESI, Figure S7) suggest that the strongly absorbing state at the lowest energy was also the emitting state for all these compounds. Then, as indicated by the corresponding Stokes shifts, larger structural reorganisations and/or solvation energy changes apparently occurred for the compounds featuring the strongest electron-releasing (X = NPh_2) or electron-withdrawing (X = NO_2) substituents, i.e., 7085 cm^{-1} and 10,685 cm^{-1} in THF, respectively (ESI, Table S1).

In line with similar studies made for **1-X, 2-X** and related derivatives [11,12,18,27], solvatochromic studies on **3-NPh_2** revealed a relatively solvent-insensitive absorption but a very solvent-sensitive emission for such a symmetrical D_{3h} molecule [47]. The shift to lower energy observed on proceeding to the most polar solvent suggests that the excited state was more polarised than the ground state. These results are consistent with the localisation of a (more polar) charge-transfer excited state on one arm of the compound (after relaxation) [14,33,48–50].

The 2PA cross-sections of these derivatives were measured in the near-IR (NIR) range (λ = 700–1000 nm) through an investigation of their two-photon excited fluorescence (TPEF). The excitation was performed with femtosecond pulses from a Ti:sapphire laser (Figure 2 and Table 2). Due to instrumental limitations (1PA below 350 nm for **3-CN**), solubility issues (**3-NO_2**), or too weak luminescence (**4**), no TPEF maxima could be detected for several samples. A comparison of these 2PA bands with the 1PA bands for each compound reveals that the 2PA maxima were situated close to twice that of the 1PA maxima detected at the lowest energy in the UV range (see ESI, Figure S9), suggesting that the excited states at the origin of 2PA in the NIR were also active for 1PA or were close in energy to the first allowed 1PA state.

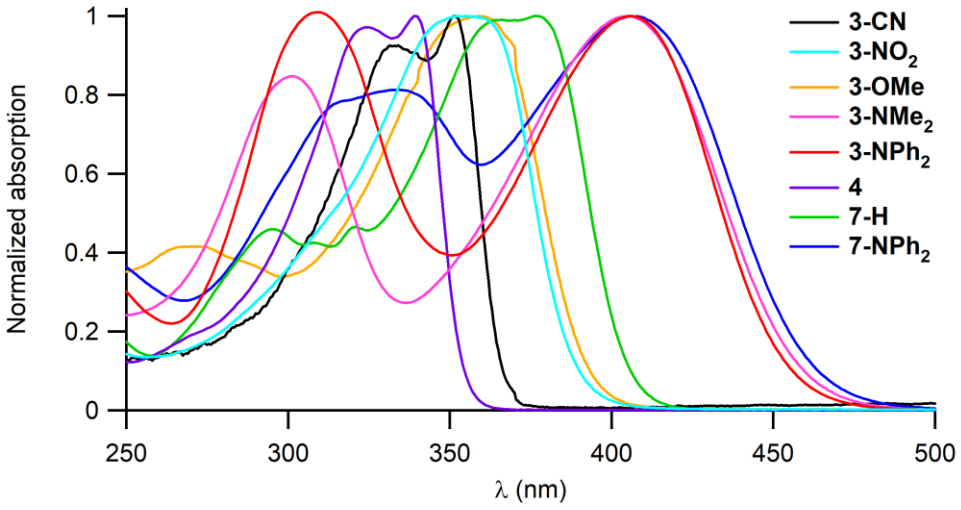

Figure 1. Normalised UV–Vis spectra for **3-X** (X = NO_2, CN, OMe, NMe_2, NPh_2), **4,** and **7-X** (X = H, NPh_2) in CH_2Cl_2 (20 °C).

Table 1. Absorption and emission properties of selected compounds **3-X**, **4**, and **7-X** in CH_2Cl_2 at 25 °C and corresponding TD-DFT computed transitions.

Cmpd	λ_{abs} (nm)	10^{-3} ε_{max} ($M^{-1}\cdot cm^{-1}$)	λ_{em} (nm)	Φ_F [a]	Stokes Shift [b] (cm^{-1})	DFT: λ_{max} (nm) [*f*] [c] in CH_2Cl_2	
						CAM-B3LYP/6-31*G [d]	MPW1PW91/6-31*G [d]
3-NO_2 [e]	355	113.0	/	n.e. [f]	/	346 [2.75]	392 [2.50]
						267 [0.04]	309 [0.13]
3-CN	352	154.0	369	0.02	1308	336 [2.88]	374 [2.59]
	332 (sh) [e]	142.0				264 [0.02]	310 [0.27]
3-OMe	359	122.0	450	0.77	5632	341 [2.64]	398 [2.04]
	270	51.0				258 [0.04]	300 [0.57]
3-NMe_2	405	105.0	587	0.27	7656	369 [2.76]	456 [1.82]
	301	89.0				263 [0.10]	340 [0.67]
3-NPh_2	406	99.0	583	0.69	7478	371 [3.03]	465 [1.83]
	309	100.0				265 [0.25]	340 [0.71]
4	339	112.0	405	0.025	4807	322 [2.43]	356 [2.15]
	270 (sh) [e]	21.3				262 [0.04]	289 [0.33]
7-H	377	173.0	455	0.80	4547	352 [3.23]	410 [2.50]
	321	67.0				270 [0.04]	325 [0.62]
	295	66.0				/	296 [0.18]
7-NPh_2	406	129.0	648	0.20	9198	375 [3.73]	483 [1.71]
	334	105.0				277 [0.32]	388 [1.20]
	317	101.0				275 [0.45]	369 [0.63]

[a] Fluorescence quantum yield in CH_2Cl_2 when excited at λ_{abs} (standard: quinine bisulphate in 0.5 M H_2SO_4). [b] Stokes shift = $(1/\lambda_{abs} - 1/\lambda_{em})$. [c] *f* = oscillator strength. [d] Functionals used. [e] Shoulder. [f] Not emissive.

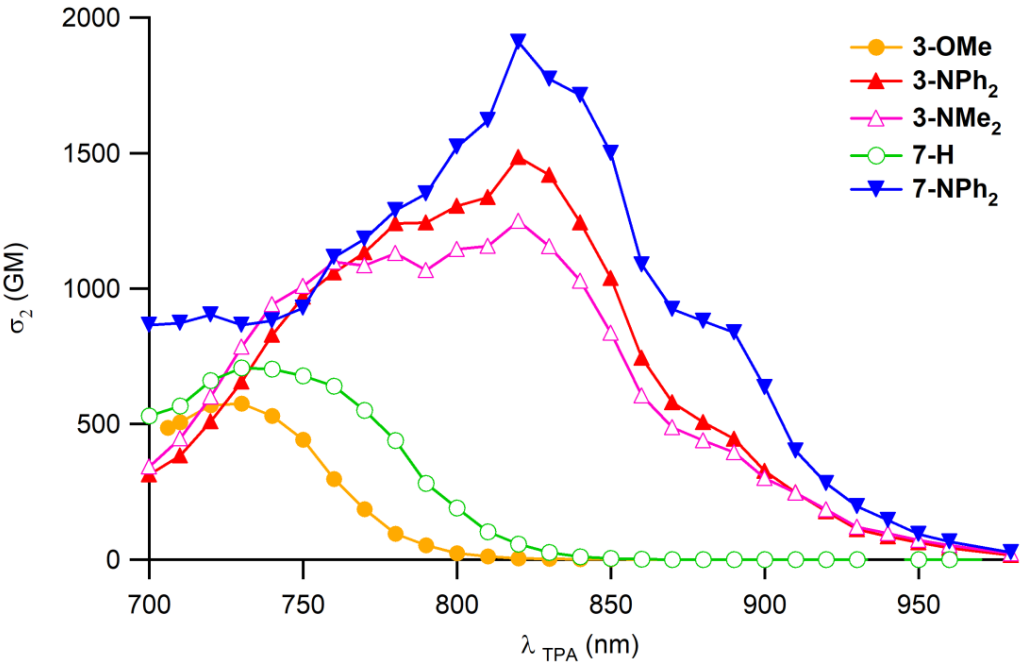

Figure 2. Two-photon absorption spectra for **3-X** (X = OMe, NMe_2, NPh_2) and **7-X** (X = H, NPh_2) in dichloromethane (20 °C).

Table 2. Experimental (TPEF) and calculated 2PA properties of selected derivatives in CH_2Cl_2 at 25 °C.

Cmpd	λ_{1PA} [a] (nm)	λ_{2PA} [b] (nm)	σ_2 [c] (GM)	σ_2/MW [d] (GM/g)	N_{eff} [e]	$\sigma_2/(N_{eff})^2$ (GM)	$\Phi_F \cdot \sigma_2$ [f] (GM)	σ_2 [λ_{2PA}] [g] (GM [nm])
3-NO_2	355	/	/	/	28.1	/	/	660 [1051]
3-CN	352	/	/	/	31.6	/	/	2735 [918]
3-OMe	359	730	580	0.830	28.1	0.732	447	5391 [954]
3-NMe_2	405	820	1250	1.694	28.1	1.579	338	8701 [1078] [h]
3-NPh_2	407	820	1500	1.351	31.8	1.488	1035	13,875 [1181]
7-H	376	730	710	0.587	38.4	0.481	568	7260 [1033]
7-NPh_2	407	820	1910	1.117	41.1	1.129	382	21,531 [1378]
1-NMe_2 [h]	352	720	360	0.458	24.5	0.600	72	4246 [800] [k]
1-NPh_2 [h]	364	740	410	0.354	28.6	0.502	300	/
2-NMe_2 [i]	357	740	380	0.517	25.0	0.609	262	4322 [800] [k]
2-NPh_2 [i]	369	760	390	0.352	29.0	0.464	285	/
6-NPh_2 [j]	383	770	500	0.284	37.8	0.350	390	/

[a] Wavelength of the one-photon absorption maximum. [b] Wavelength of the two-photon absorption maximum. [c] 2PA cross-section at λ_{2PA}. [d] Specific cross-sections: figure-of-merit relevant for applications in optical limiting or nanofabrication [51]. [e] Effective number of π electrons [52]. [f] Two-photon brightness: figure-of-merit for imaging applications [51]. In these expressions, Φ_F represents the luminescence quantum yield and *MW* the molecular weight. [g] Computed values using the SAOP functional (see text). [h] For exp. data, see also [11]. [i] For exp. data, see also [12] [j] For exp. data, see also [33]. [k] See: [53].

To understand better the structural dependence of these nonlinear absorptions on the π electrons, we divided their 2PA cross-sections by the square of the effective number of π electrons (N_{eff}^2) [54]. These figures of merit (σ_2/N_{eff}^2) allow normalisation of the cross-sections and should permit a better comparison between them regardless of the different number of π electrons in each compound (see Section 3) [54]. The N_{eff} values were derived according to the method initially proposed by Kuzyk [52], by decomposing the various compounds into a collection of "independently" conjugated π manifolds (ESI, Figure S18).

2.3. Density Functional Theory (DFT) Calculations

DFT calculations (see computational details in Section 4.4) were performed on the **3-X** (X = NO_2, CN, H, OMe, NMe_2, NPh_2), **4** and **7-X** (X = H, NPh_2) derivatives. Similar computations were also performed on the model compounds **9a-b**, **10a-b**, and **11a-b** (Scheme 3) to specifically investigate the impact of the central core on the electronic structure of **1-X**, **2-X**, and **3-X** analogues. The key results of these are disclosed in the next section.

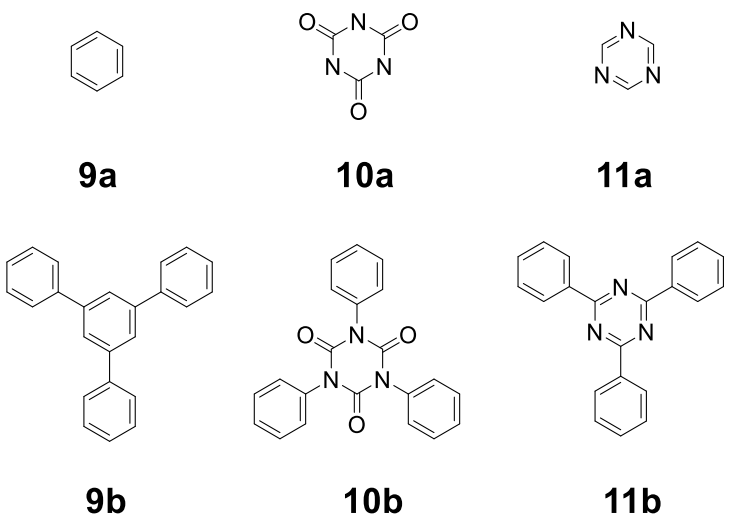

Scheme 3. Model compounds studied for investigating the changes occurring in the FMO when changing the central core.

All derivatives adopted a nearly coplanar conformation after geometrical optimisation relative to the central core upon geometry optimisation in CH_2Cl_2 (ESI, Table S1). As a result, in line with the available crystallographic data for **3-CN** [17] or **3-NPh$_2$**, **3-X** compounds appeared significantly more planar in solution than their **1-X** or **2-X** analogues (55–80°) [18]. Such planar conformations are likely favoured by weak intramolecular hydrogen bonds between *ortho* hydrogen atoms of the first aromatic ring and the triazine nitrogen atoms (with N···H- distances around 2.46 Å in optimised structures) [55,56]. Thus, the permanent dipole moment of **3-X** and **4** compounds with axially symmetric X substituents was nearly zero (ESI, Table S2) [11,33].

The HOMO–LUMO gap in these derivatives (Table 3) was smaller than that in the corresponding isocyanurate (**1-X**) and triphenylbenzene (**2-X**) analogues. Starting from **3-CN**, the calculations revealed that this gap progressively decreased when increasingly electron-releasing substituents were installed at their periphery, mirroring the trend observed experimentally for the lowest-lying intense absorptions of these compounds (Table 1). In line with experimental observations (Figure 1), replacing the peripheral 1,4-phenylene groups with a 2,7-fluorenyl one in **3-X**, when a strong electron-releasing X group such as X = NPh_2 was present (Figure 3), led only to a slight bathochromic shift of the first allowed absorption band computed at lowest energy for **7-X** (e.g., 371 nm (f = 3.03) for **3-NPh$_2$** vs. 375 nm (f = 3.73) for **7-NPh$_2$**, using CAM-B3LYP). In contrast, computations predicted that a much more pronounced shift could be expected for a less electron-releasing substituent such as X = H (e.g., 329 nm (f = 2.46) for **3-H** vs. 352 nm (f = 3.23) for **7-H**, using the same functional), reminiscent of observations previously made between **1-X** and **6-X** [33]. Calculations made for **3-X** compounds also indicated that, for X = CN (ESI; Figure S14) and more electron-withdrawing substituents, the direction of the photo-induced charge-transfer process was reversed, leading to a "umpolung" of the polarisation of the peripheral branches in the first allowed excited state, as already observed for the **2-X** analogues [12].

Table 3. Calculated (CAM-B3LYP/6-31G* level in CH_2Cl_2) HOMO–LUMO energy gaps in CH_2Cl_2 for **1-X**, **2-X**, and **3-X**.

X	HOMO–LUMO Gap (eV)		
	2-X	**1-X**	**3-X**
NO_2	5.62	7.06	5.82
CN	6.09	6.45	5.99
H	6.42	7.47	6.00
OMe	6.23	6.30	5.71
NMe_2	5.81	5.86	5.18
NPh_2	5.70	5.82	5.11

TD-DFT calculations qualitatively reproduced the energy trends observed for the most intense transitions at the lowest energy for **3-X**, **4**, and **7-X** (Table 1). Transition energies were consistently overestimated when using the CAM-B3LYP functional and underestimated when using the MPW1PW91 functional [57], a better agreement with the experiment being obtained using the CAM-B3LYP functional for the low energy band [58]. However, overall, better results were obtained with MPW1PW91 when the transition moments were also considered (ESI, Figure S13). The nature of the dominant excitations underlying the first absorption band (ESI, Table S4) was the same using either the CAM-B3LYP or the MPW1PW91 functional. It does not change much for all the compounds presently considered. These excitations are a pair of (nearly) degenerate transitions that would correspond to the set of degenerate transitions towards an E-type excited state under strict C_{3v} symmetry (i.e., an $E \leftarrow A$ transition). In line with previous findings for **1-X** and **2-X** [11,12,33], the first absorption band, therefore, corresponds to a $\pi \rightarrow \pi^*$ symmetric charge transfer (CT) between the peripheral arms and the central core.

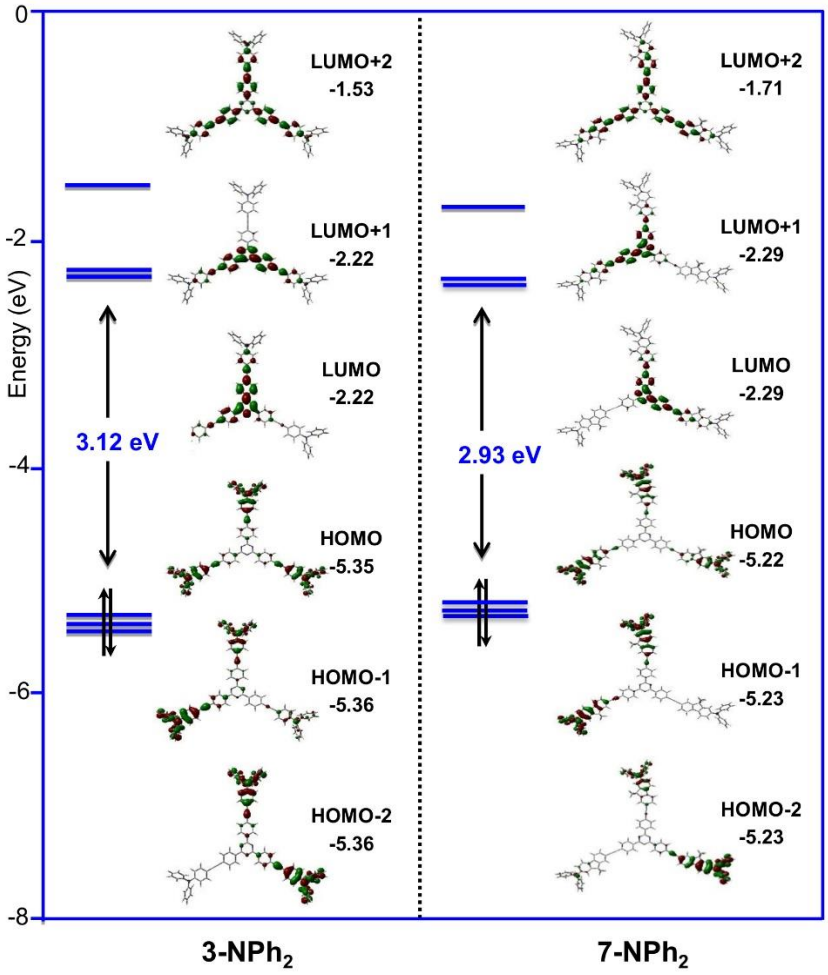

Figure 3. Frontier molecular orbitals involved in the lowest-energy (intense) allowed transition for **3-NPh$_2$** and **7-NPh$_2$** (isocontour 0.02 [e/bohr^3]$^{1/2}$).

Consistent with the acceptor character of the s-triazine ring, the CT occurs usually from the periphery towards the centre for all compounds, when X is electron-releasing [11,12,33]. The next and weaker absorption at higher energy observed for all these derivatives also corresponds to an allowed π–π* transition with a similar CT character but involves deeper-lying occupied MOs. As a result, this transition is more arm-centred than that at the lowest energy. However, it does not correspond to an n–π* transition, as previously proposed [18]. Indeed, according to our calculations, transitions with n–π* character were much weaker (f < 0.1) and remained hidden beneath the dominant bands at lowest energy (especially for **7-X** derivatives) but also at higher energy.

In line with our previous studies [53,59], the simulations of 2PA spectra were also carried out for selected compounds using the damped cubic response theory of Jensen et al. [60]. The calculations were performed using the SAOP functional, for sake of consistency with previous computations already reported on these compounds (see computational details in Section 4.5) [53]. The simulated 2PA spectra (ESI, Figure S17) revealed a first 2PA band for these compounds at lower energy than that experimentally determined with significantly higher 2PA cross-section values (Table 2). While an overestimation of the real 2PA cross-sections by this method was expected [53], the experimental trends were generally qualitatively fairly well reproduced within a given family of compounds [59]. Based on these SAOP calculations, we speculate that the cross-section of the first 2PA band of **3-CN** or **3-NO$_2$**, which could not be experimentally determined, should be lower than that of the other **3-X** compounds. Interestingly, these computations revealed the existence

of another and much larger 2PA peak at about 620 nm for **3-NPh$_2$**. This second 2PA band was hypsochromically shifted for **3-NMe$_2$** and **3-OMe**.

3. Discussion

As for their **1-X** and **2-X** analogues [12,33], the first allowed electronic transition at lowest energy for most of the **3-X** compounds corresponds to a $\pi \rightarrow \pi^*$ transition, with a charge transfer (CT) character directed from the electron-rich peripheral arms towards the central electron-poor core (Figure 3). In line with previous investigations on **1-X** [11,33] and **2-X** [4,14] derivatives, the available solvatochromic studies on some of these molecules [18,27] strongly suggest localisation of the excited state on one branch in the first excited state after vibrational relaxation. As surmised at the start of this study, DFT calculations on compounds **9a-b**, **10a-b**, and **11a-b** (Figure 4), confirm that the s-triazine central unit in **3-X** compounds is more electron-withdrawing than the isocyanurate core in **1-X** analogues. Indeed, regardless of the presence of three peripheral phenyl groups (**11b**) or not (**11a**), for a HOMO of comparable energy, the LUMO is always more stabilised in **11a-b** than in **10a-b**, resulting in lower HOMO–LUMO gaps for the triazine-cored compounds relative to their isocyanurate analogues.

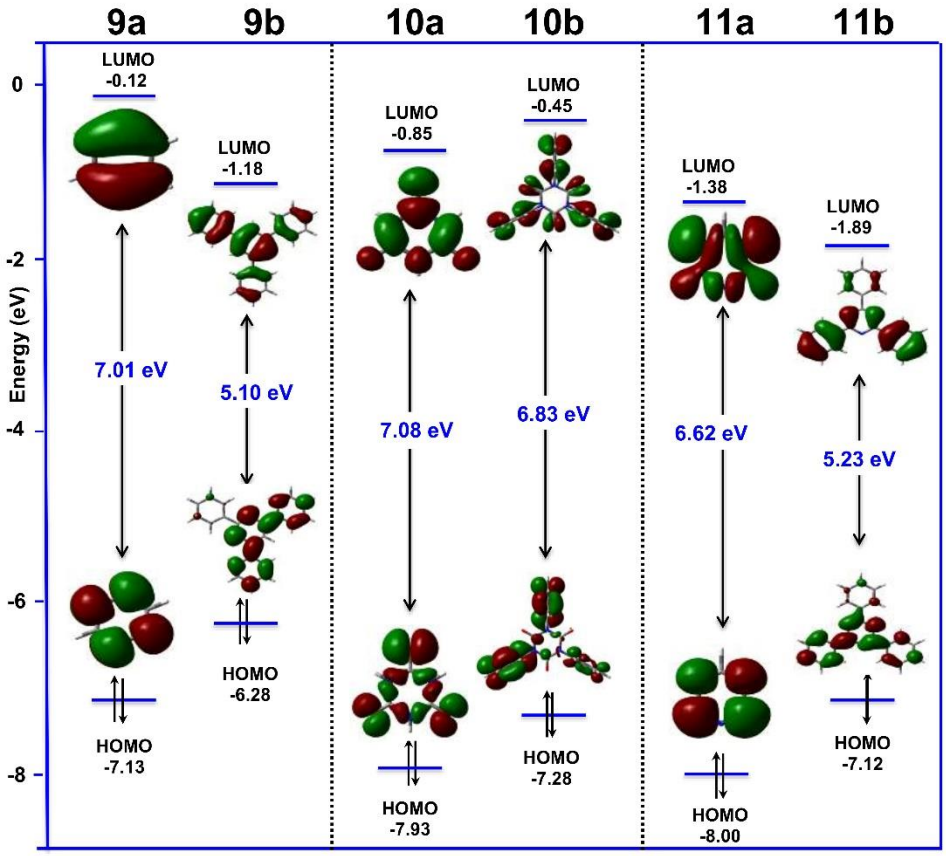

Figure 4. Frontier molecular orbitals of the **9a-11a** and **9b-11b** compounds modelling the central core in **2-X**, **1-X** and **3-X** (isocontour 0.02 [e/bohr^3]$^{1/2}$).

Furthermore, **3-X** compounds were also significantly more fluorescent than their **1-X** counterparts, a trend especially apparent with the weaker electron-releasing substituents (X = OMe, NMe$_2$). As for **2-X** derivatives, this might be related to the stronger transition moments observed for the lowest-energy 1PA absorptions in **3-X** compared with **1-X** analogues. Stronger transition moments should result in larger emission quantum yields, owing to the Strickler–Berg relationship [61], and in the absence of low-lying n–π^* states able to efficiently quench the fluorescence in **3-X** derivatives [11,62].

As previously observed for 1,3,5-triphenylbenzene- or isocyanurate-cored families of analogues, electron-releasing peripheral (X) substituents favour larger 2PA cross-sections (σ_2) [11,12]. Thus, the cross-sections determined by TPEF for the **3-X** derivatives were always significantly higher than those found for **1-X** and **2-X** (Table 2). In accordance with this observation, the σ_2 values calculated for **3-NMe$_2$** and for quite all other **3-X** derivatives (except for X = CN) were also higher than those previously computed for **1-NMe$_2$** or **2-NMe$_2$** (Table 2) [53]. In spite of the fact that SAOP calculations always overestimate 2PA cross-sections [53,59], the present study therefore provides further evidence that the qualitative ordering of the experimental σ_2 values is generally retrieved.

Then, the 2PA cross-section presently measured for **7-H** (710 GM) is significantly lower than the value of 2210 GM independently reported for its dihexyl analogue (**13-H**; Scheme 4) at nearly the same wavelength (730 nm vs. 740 nm) [27,63]. Actually, the value reported for **7-H** is closer to that reported for compound **14** (395 GM at 790 nm), although the latter value was not recorded at the TPA peak maximum (779 nm) and possibly includes some RSA contribution [64].

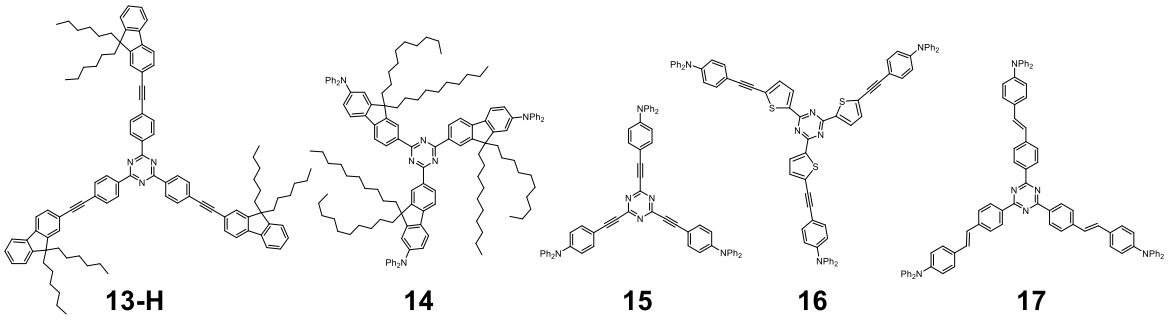

Scheme 4. Related derivative independently reported.

Comparison of the photophysical data presently measured for **3-NPh$_2$** with those reported for structurally related s-triazine derivatives such as **15** [19], **16** [22], and **17** [29] (Scheme 4) revealed larger fluorescence yields in chlorinated organic solvents for **3-NPh$_2$** (69% for the latter compound vs. 52%, 51%, and 27%, respectively). Regarding 2PA, removing the first 1,4-phenyl ring significantly reduced the 2PA cross-section (1500 GM for **3-NPh$_2$** vs. 910 GM reported for **15**), while replacing it with a 2,5-thienyl unit apparently did not impact this figure significantly (1508 GM reported for **16**) apart from slightly red-shifting the 2PA maximum (850 nm vs. 830 nm for **3-NPh$_2$**). Then, changing the alkynyl linkers for alkenyl ones in **3-NPh$_2$** seemed to reduce the 2PA cross-section. However, care should be given here since the value reported for **17** (495 GM) was obtained at a single wavelength (800 nm) which did not exactly match that of the 2PA maximum of this compound.

In terms of NLO activity per volume/mass unit, specific cross-sections [51] (Table 2) revealed that **3-X** derivatives are much more active than **1-X** and **2-X** (Table 2). More precisely, among all triazine derivatives investigated, **3-NPh$_2$** appears to be the best-suited two-photon absorber for elaborating molecular materials. As confirmed by other relevant figures of merit ($\sigma_2/(N_{\text{eff}})^2$) [54], these compounds optimise 2PA for a given number of effective electrons (N_{eff}), a feature possibly connected to their enforced planarity [65] but also certainly to their more pronounced (multi)polarity, compared to those of their **1-X** and **2-X** analogues. Both of these features ultimately translate into lower HOMO–LUMO gaps for **3-X** derivatives. Based on a simple perturbational approach, such a reduction in HOMO–LUMO gaps when progressing from **1-X** or **2-X** to **3-X** derivatives is expected to favour 2PA (at least at wavelengths above that of the lowest-energy absorption) [9]. Finally, the near-perfect spectral overlap between the 1PA spectrum plotted at half wavelength and the 2PA spectrum for each of these octupolar compounds (ESI, Figure S9) suggests a near degeneracy of the *A* and *E* excited states, in line with a small electronic/excitonic coupling

between the peripheral branches [5,14,66]. As a result, the contribution of the octupolar symmetry to the 2PA improvement in these compounds should not be determining [67,68].

In terms of applied uses of these 2PA absorbers, both the significant bathochromic shift of 1PA and 2PA peaks and the larger intensity of the first absorption band result in a diminished transparency relative to **1-X** analogues, making them less favourable for selected NLO applications [6] such as optical limiting [69] or second harmonic generation in the visible range [70]. However, both the increased two-photon brightness [51] and the bathochromically-shifted 2PA maxima for the various **3-X** compounds (Table 2) points to a larger potential for two-photon fluorescence imaging. Such uses were already reported for structurally different s-triazine derivatives presenting much poorer figures of merit than **3-X** [71], but also for nanoparticles obtained from extended analogues of **17**, and giving rise to aggregation-induced emission (AIE) in water–THF mixtures [30]. Compared with **1-X** or **2-X** derivatives, the best candidate for fluorescence imaging is **3-NPh$_2$**. This compound has indeed a two-photon brightness far above those of its known triphenylbenzene and isocyanurate analogues (**1-NPh$_2$** and **2-NPh$_2$**, respectively) and a 2PA peak at 820 nm, i.e., also significantly bathochromically shifted relative to them (Table 2) [6,9]. In contrast, contrary to the trend previously observed with triarylisocyanurates derivatives [33], the tris(2-fluorenyl)triazine **7-NPh$_2$** presents neither a higher 2PA cross-section value nor a larger two-photon brightness than **3-NPh$_2$**.

4. Materials and Methods

4.1. General

All manipulations were carried out under an inert atmosphere of argon with dried and freshly distilled solvents [72]. Transmittance FTIR spectra were recorded using a Perkin Elmer Spectrum 100 spectrometer (Waltham, MA, USA) equipped with a universal ATR sampling accessory (400–4000 cm^{-1}). Raman spectra of the solid samples were obtained by diffuse scattering on a Bruker IFS 28 spectrometer and recorded in the 400–2500 cm^{-1} range (Stokes emission), with a laser excitation source at 1064 nm or on a Raman LabRAM HR 800 spectrometer with a laser excitation source at 785 nm. Nuclear magnetic resonance spectroscopy was performed using a Bruker AV-300 (300 MHz for ^{1}H, 75 MHz for ^{13}C) a Bruker AV-400 (400 MHz for ^{1}H, 101 MHz for ^{13}C) or a Bruker AV–500 (500 MHz for ^{1}H, 101 MHz for ^{13}C) spectrometers at ambient temperature. ^{1}H and ^{13}C spectra were calibrated using residual solvent peaks [73,74]. MS analyses were performed at the "Centre Regional de Mesures Physiques de l'Ouest" (CRMPO, Université de Rennes) on high resolution Bruker Maxis 4G or Thermo Fisher Q-Extractive Spectrometers. Elemental analyses were also performed at CRMPO. Chromatographic separations (rapid suction filtration (RSF), column chromatography, or flash chromatography) were performed on Merck silica gel (40–63 µm), Aldrich basic Alumina (act 1), or Aldrich neutral Alumina (act 1), with the eluants indicated. Commercial reagents and (pre/co)catalysts were used as received. The trisbromo s-triazine precursor **8-Br** was synthesised using a procedure inspired by the literature [42], which was subsequently extended to the known trisiodo analogue **8-I** (ESI). The triyne **8-C≡CH** was also obtained following modifications of the reported literature procedure (ESI) [16]. The known triazine derivatives **3-CN** [17], **3-OMe** [15], and **3-NPh$_2$** [18] were obtained according to published procedures and fully characterised (ESI), as were the required alkynes [33,75–78].

4.2. Synthesis of the New Triazine Compounds

2,4,6-tris{4′-[(4″-dimethylamino)-2‴-phenylethynyl]phenyl}-1,3,5-triazine (3-NMe$_2$). A dry Schlenk flask was charged with **8-I** (203 mg, 0.295 mmol), 4-ethynyl-*N*,*N*-dimethylaniline (211 mg, 1.453 mmol, 5 eq.), Pd(PPh$_3$)$_4$ (35 mg, 0.030 mmol, 10 mol%), and CuI (11 mg, 0.058 mmol, 20 mol%), and then degassed (4 × vacuum/argon cycles). A degassed mixture of DMF/^{i}Pr$_2$NH (2/1 mixture, 30 mL) was added using a cannula, and the flask was sealed and heated at 50 °C for 2 days. The solvent was removed in vacuo and the residue triturated with Et$_2$O to remove the unreacted starting material. The residue was dissolved in a mix-

ture of pentane/CH_2Cl_2/NEt_3 (200 mL/200 mL/20 mL) and filtered through a short plug (2 cm × 2 cm) of neutral alumina (deactivated with NEt_3). The bright orange filtrate was evaporated under reduced pressure, giving the title product as an orange powder (141 mg, 65%). **MP:** > 150 °C (dec.). R_f: 0.38 (petroleum ether/CH_2Cl_2 [7:3]). **HRMS (ESI, MeOH):** m/z = 739.3542 $[M + H]^+$ (calc. for $C_{51}H_{43}N_6$: 739.3544). **Anal. Calc. for $C_{51}H_{42}N_6 \bullet H_2O$:** C, 80.92, H, 5.86, N, 11.10; found: C, 81.39, H, 6.25, N, 10.24. **^{1}H NMR (500 MHz, $CDCl_3$):** δ 8.74 (d, *J* = 8.4 Hz, 6H, H_{Ph}); 7.69 (d, *J* = 8.4 Hz, 6H, H_{Ph}); 7.48 (d, *J* = 8.8 Hz, 6H, $H_{Ph'}$); 6.71 (d, *J* = 8.0 Hz, 6H, $H_{Ph'}$); 3.02 (s, 18H, CH_3). **^{13}C{^{1}H} NMR (126 MHz, $CDCl_3$):** δ = 171.2 ($C_{triazine}$); 135.1 ($C_{Ph'}$); 133.1 ($C_{Ph}H$); 131.6 ($C_{Ph'}H$); 130.6 (C_{Ph}); 129.0 ($C_{Ph}H$); 128.7 (C_{Ph}); 125.7 ($C_{Ph'}H$); 112.0 ($C_{Ph'}H$); 94.1 (C≡*C*); 87.9 (*C*≡C); 40.4 (*C*H$_3$). **IR (KBr, cm^{-1}):** $\overline{\upsilon}$ = 2849 (w, C_{Ar}-H); 2201 (m, C≡C); 1598 (s, C=C_{Ar}); 1566 (m, C=C_{Ar}); 1507 (vs, C=$N_{triazine}$). **Raman (neat, cm^{-1}):** $\overline{\upsilon}$ = 2205 (s, C≡C); 1600 (vs, C=C_{Ar}); 1511 (m, C=$N_{triazine}$); 990 (w, C=$N_{triazine}$).

2,4,6-tris{4′-[(4′′-nitro)-2′′′-phenylethynyl]phenyl}-1,3,5-triazine (3-NO$_2$). The compound was isolated using a workup similar than that described above from **8-C≡CH** (110 mg, 0.289 mmol) and 4-bromonitrobenzene in excess (293 mg, 1.45 mmol, 5 eq.) with $Pd(PPh_3)_4$ (10 mol%) and CuI (20 mol%) as catalysts in an DMF/NEt_3 mixture at 75 °C for 2.5 days. The volatiles were removed in vacuo and the residue triturated with small portions of CH_2Cl_2 and Et_2O to remove the unreacted 4-bromonitrobenzene and other soluble byproducts that formed during the reaction. The residue (ca. 90 mgs) was then dissolved in THF and filtered through a short plug (2 cm × 2 cm) and recrystallised several times to eventually yield pure fractions of yellow product that were used for characterisations. **MP:** > 250 °C (dec.). R_f: 0.65 (petroleum ether/THF [9:1]). **HRMS (MALDI-TOF, DTCB):** m/z = 745.183 $[M + H]^+$ (calc. for $C_{45}H_{25}N_6O_6$: 745.18301). **^{1}H NMR (300 MHz, THF-d_8):** δ = 8.90 (d, *J* = 8.7 Hz, AA′XX, 6H, $H_{Ph'}$); 8.31 (d, *J* = 8.7 Hz, AA′XX, 6H, H_{Ph}); 7.83 (m, 12H, $H_{Ph'}$). **^{13}C{^{1}H} NMR (125 MHz, THF-d_8):** δ = 172.2 ($C_{triazine}$); 148.8 ($C_{Ph'}$); 137.6 (C_{Ph}); 133.6 ($C_{Ph'}H$); 133.1 ($C_{Ph}H$); 130.4 (C_{Ph}); 130.2 ($C_{Ph}H$); 127.8 ($C_{Ph'}$); 124.8 ($C_{Ph'}H$); 94.4 (C≡*C*); 91.3 (*C*≡C). **IR (KBr, cm^{-1}):** $\overline{\upsilon}$ = 2213 (w, C≡C); 1592 (s, C=C_{Ar}); 1569 (m, C=C_{Ar}); 1510 (vs, $NO_{2\text{-sym}}$); 1506 (vs, C=$N_{triazine}$); 1340 (vs, $NO_{2\text{-asym}}$). **Raman (neat, cm^{-1}):** $\overline{\upsilon}$ = 2217 (vs, C≡C); 1600 (vs, C=C_{Ar}); 1510 (m, C=N_{triaz}); 1341 (m, $NO_{2\text{-asym}}$); 990 (w, C=$N_{triazine}$).

2,4,6-tris{4′-[2′′′-(4′′-pyridyl)ethynyl]phenyl}-1,3,5-triazine (4). A solution of TBAF (1.0 M in THF, 0.2 mL, 0.2 mmol) was evaporated to dryness in a dry Schlenk flask. The flask was then charged with **8-I** (394 mg, 0.57 mmol), (trimethylsilyl)ethnynyl pyridine (566 mg, 3.23 mmol), $Pd(PPh_3)_4$ (78 mg, 0.067 mmol) and CuI (23 mg, 0.121 mmol) and then degassed (4 × vacuum/argon cycles). The flask was wrapped in foil before degassed DMF (20 mL) and NEt_3 (9 mL) were added using a cannula. The reaction mixture was then stirred at 25 °C for 2 days. The solvent was removed in vacuo, and the residue was dissolved in CH_2Cl_2 (100 mL), washed with water (3 × 50 mL), and dried ($MgSO_4$). The solvent was removed under reduced pressure, and the crude material purified using column chromatography (neutral alumina, 5 cm × 6 cm, eluting with a methanol/CH_2Cl_2 [2:98] mixture). The resulting solid was then precipitated from methanol/CH_2Cl_2, with the slow evaporation of the CH_2Cl_2, and collected on a glass frit, washed with methanol, and dried under reduced pressure (high vacuum) for 12 h giving the title product as an off-white coloured powder (261 mg, 75%). **MP:** 310 °C (dec.). R_f: 0.60 (MeOH/CH_2Cl_2 [2.5:97.5]). **HRMS (ESI, MeOH):** m/z = 613.2134 $[M + H]^+$ (calc. for $C_{42}H_{25}N_6$: 613.2135). **Anal. Calc. for $C_{42}H_{24}N_6 \bullet ½H_2O$:** C, 77.91, H, 3.85, N, 12.83; found: C, 78.35, H, 3.80, N, 12.89. **^{1}H NMR (400 MHz, CD_2Cl_2):** δ = 8.76 (d, *J* = 8.2 Hz, 6H, H_{Ph}); 8.61 (d, *J* = 5.6 Hz, 6H, $H_{Ph'}$); 7.76 (d, *J* = 8.2 Hz, 6H, H_{Ph}); 7.44 (d, *J* = 5.6 Hz, 6H, $H_{Ph'}$). **^{13}C{^{1}H} NMR (101 MHz, CD_2Cl_2):** δ = 171.6 ($C_{triazine}$); 150.5 ($C_{Py}H$); 136.9 (C_{Ph}); 132.7 ($C_{Ph}H$); 131.4 (C_{Py}); 129.5 ($C_{Ph}H$); 127.0 (C_{Ph}); 126.1 ($C_{Py}H$); 93.6 (C≡*C*); 89.8 (*C*≡C). **IR (KBr, cm^{-1}):** $\overline{\upsilon}$ = 2218 (w, C≡C); 1598 & 1569 (m, C=C_{Ar}); 1515 (vs, C=$N_{triazine}$). **Raman (neat, cm^{-1}):** $\overline{\upsilon}$ = 2223 (s, C≡C); 1605 (vs, C=C_{Ar}); 1520 (w, C=$N_{triazine}$); 992 (w, C=$N_{triazine}$).

2,4,6-tris{4′-[2′′′-(9′′,9′′-dibutyl-2′′-fluorenyl)ethynyl]-phenyl}-1,3,5-triazine (7-H). A dry Schlenk flask was charged with **8-Br** (100 mg, 0.183 mmol), 2-ethynyl-9,9-dibutylfluo rene (263 mg, 0.869 mmol), $Pd(PPh_3)_4$ (24 mg, 0.021 mmol), and CuI (8 mg, 0.042), and

then degassed (4 × vacuum/argon cycles). A mixture of dry, degassed DMF/$^{i}Pr_2NH$ (1/1 mixture, 30 mL) was added using a cannula. The flask was sealed and the reaction mixture was heated at 70 °C for 3 days. The solvent was removed in vacuo, and the residue was dissolved in CH_2Cl_2 (100 mL), washed with water (3 × 30 mL) and dried ($MgSO_4$). The solvent was removed under reduced pressure, and the crude material was purified using flash column chromatography (silica gel, 3.5 cm × 15 cm, eluting with an hexanes/CH_2Cl_2 [9:1] mixture), giving the title product as a pale yellow solid (198 mg, 89%). **MP:** 146 °C. R_f: 0.52 (petroleum ether/CH_2Cl_2 [85:15]). **HRMS (ESI, MeOH):** m/z = 1210.6970 $[M + H]^+$ (calc. for $C_{90}H_{88}N_3$: 1210.6973). **Anal. Calc. for $C_{90}H_{87}N_3$:** C, 89.29, H, 7.24, N, 3.47; found: C, 89.33, H, 7.54, N, 3.50. **^{1}H NMR (400 MHz, $CDCl_3$):** δ = 8.80 (d, *J* = 8.4 Hz, 6H, H_{Ph}); 7.79 (d, *J* = 8.4 Hz, 6H, H_{Ph}); 7.73–7.71 (m, 6H, H_{Flu}); 7.61–7.58 (m, 6H, H_{Flu}); 7.36–7.35 (m, 9H, H_{Flu}); 2.02 (t, *J* = 8.0 Hz, 12H, C$H_{2\text{-}Bu}$); 1.16–1.07 (m, 12H, C$H_{2\text{-}Bu}$); 0.70 (t, *J* = 7.4 Hz, 18H, C$H_{3\text{-}Bu}$); 0.66–0.50 (m, 12H, C$H_{2\text{-}Bu}$). **^{13}C{^{1}H} NMR (101 MHz, $CDCl_3$):** δ = 171.3 ($C_{triazine}$); 151.2; 151.0 (C_{Flu}); 142.0; 140.5; 135.7; 132.0; 131.0; 129.1; 128.0; 127.8; 127.1; 126.2; 123.1; 121.1; 120.2; 119.9; 93.78 (C≡*C*); 89.5 (*C*≡C); 55.3 (C_{Flu}); 40.4 (*C*$H_{2\text{-}Bu}$); 26.1 (*C*$H_{2\text{-}Bu}$); 23.2 (*C*$H_{2.\text{-}Bu}$); 14.0 (*C*$H_{3.\text{-}Bu}$). **IR (KBr, cm^{-1}):** $\overline{\upsilon}$ = 2953, 2925, 2854 (m, C_{Ar}-H); 2196 (w, C≡C); 1603 (m, C=C_{Ar}); 1569 (s, C=C_{Ar}); 1507 (vs, C=$N_{triazine}$). **Raman (neat, cm^{-1}):** $\overline{\upsilon}$ = 2202 (s, C≡C); 1605 (vs, C=C_{Ar}); 1511 (w, C=$N_{triazine}$); 991 (vw, C=$N_{triazine}$).

2,4,6-tris{4′-[2‴-(9″,9″-dibutyl-7″-diphenylamino-2″-fluorenyl)ethynyl]phenyl}-1,3,5-triazine (7-NPh$_2$). A dry Schlenk flask was charged with **8-Br** (49 mg, 0.090 mmol), 2-ethynyl-9,9-dibutyl-7-diphenylaminofluorene (198 mg, 0.422 mmol), $Pd(PPh_3)_4$ (11 mg, 0.009 mmol), and CuI (4 mg, 0.020 mmol), and then degassed (3 × vacuum/argon cycles). A mixture of dry, degassed DMF/$^{i}Pr_2NH$ (2/1 mixture, 20 mL) was added using a cannula. The flask was sealed, and the reaction mixture was heated at 70 °C for 2.5 days. The solvent was removed in vacuo, and the residue was dissolved in CH_2Cl_2 (70 mL), washed with water (2 × 20 mL), and dried ($MgSO_4$). The solvent was removed under reduced pressure, and the crude material was purified using flash column chromatography (neutral alumina deactivated with NEt_3, eluting with mixture of ether/hexanes/NEt_3 gradient from 50/450/5 mL up to 245/250/5 mL mixture), giving the title product as a bright yellow waxy solid (27 mg, 18%). **MP:** 140 °C (dec.). R_f: 0.34 (petroleum ether/CH_2Cl_2 [7:3]). **HRMS (ESI, $CHCl_3$/MeOH [8:2]):** m/z = 855.4542 $[M]^{2+}$ (calc. for $C_{126}H_{114}N_6$: 855.4547). **Anal. Calc. for $C_{126}H_{114}N_6$•½CH_2Cl_2:** C, 86.58, H, 6.61, N, 4.79; found: C, 86.72, H, 6.89, N, 4.87. **^{1}H NMR (400 MHz, $CDCl_3$):** δ = 8.81 (d, *J* = 8.6 Hz, AA′XX′, 6H, H_{Ph}); 7.80 (d, *J* = 8.6 Hz, AA′XX′, 6H, H_{Ph}); 7.65–7.55 (m, 12H, H_{Flu}); 7.32–7.25 (m, 12H, H_{Ph2N}); 7.19–7.14 (m, 15H, H_{Ph2N} and H_{Ph2N}); 7.08–7.03 (m, 9H, H_{Ph2N} and H_{Ph2N}); 1.92 (m, 12H, C$H_{2\text{-}Bu}$); 1.13 (m, 12H, C$H_{2\text{-}Bu}$); 0.80–0.65 (m, 30H, C$H_{3\text{-}Bu}$ & C$H_{2\text{-}Bu}$). **^{1}H NMR (400 MHz, $CDCl_3$):** δ = 171.3 ($C_{triazine}$); 152.8; 150.9 (C_{Flu}); 148.0; 147.9; 141.9; 135.6; 135.5; 131.9; 131.1; 129.4; 129.1; 128.1; 126.1; 124.2; 123.4; 122.9; 120.9; 120.3; 119.2; 119.1; 93.8 (C≡*C*); 89.4 (*C*≡C); 55.2 (C_{Flu}); 40.1 (*C*$H_{2\text{-}Bu}$); 26.2 (*C*$H_{2\text{-}Bu}$); 23.2 (*C*$H_{2\text{-}Bu}$); 14.0 (*C*$H_{3.\text{-}Bu}$). **IR (KBr, cm^{-1}):** $\overline{\upsilon}$ = 2194 (w, C≡C); 1593 (s, C=C_{Ar}); 1569 (s, C=C_{Ar}); 1508 (vs, C=$N_{triazine}$); 1490 (vs, C=$N_{triazine}$). **Raman (neat, cm^{-1}):** $\overline{\upsilon}$ = 2199 (w, C≡C); 1601 (vs, C=C_{Ar}); 1569 (w, C=C_{Ar}); 1508 (w, C=$N_{triazine}$); 989 (w, C=$N_{triazine}$).

4.3. Fluorescence Measurements

All photophysical measurements were performed with freshly prepared air-equilibrated CH_2Cl_2 (or THF) solutions (HPLC grade) at room temperature (298 K). UV–Vis absorption spectra were recorded on dilute solutions (ca. 10^{-5} M) by using a Jasco V-570 spectrophotometer (Mary's Court, Easton MD, USA). The samples used to make the solutions were freshly recrystallised or thoroughly washed with cooled ether/pentane prior to the measurements to remove any organic impurity. Steady-state fluorescence studies were performed in diluted air-equilibrated solutions in quartz cells of 1 cm path length (ca. 1×10^{-6} M, optical density < 0.1) at room temperature (20 °C), using an Edinburgh Instruments (FLS920) spectrometer (Edinburgh, UK) in photon-counting mode. Fully corrected excitation and emission spectra were obtained, with an optical density at $\lambda_{exc} \leq 0.1$. The

fluorescence quantum yield of each compound was calculated using the integral of the fully corrected emission spectra relative to a standard, quinine bisulphate (QBS, λ_{ex} = 346 nm, Φ_F = 0.546) [79,80]. UV–Vis absorption spectra used for the calculation of the fluorescence quantum yields were recorded using a double-beam Jasco V-570 spectrometer.

4.4. Two-Photon Absorption Experiments

To span the 790–920 nm range, an Nd:YLF-pumped Ti:sapphire oscillator (Chameleon Ultra, Coherent) was used, generating 140 fs pulses at an 80 MHz rate. The excitation power was controlled using neutral density filters of varying optical density mounted in a computer-controlled filter wheel. After a fivefold expansion through two achromatic doublets, the laser beam was focused with a microscope objective (10×, NA 0.25, Olympus, Shinjuku, Tokyo, Japan) into a standard 1 cm absorption cuvette containing the sample. The applied average laser power arriving at the sample was typically between 0.5 and 40 mW, leading to a time-averaged light flux in the focal volume on the order of 0.1–10 mW/mm^2. The fluorescence intensity was measured at several excitation powers in this range owing to the filter wheel. For each sample and each wavelength, the quadratic dependence of the fluorescence intensity (F) on the excitation intensity (P), i.e., the linear dependence of F on P^2 was systematically checked (see ESI, Figure S8). The fluorescence from the sample was collected in epifluorescence mode, using the microscope objective, and reflected by a dichroic mirror (Chroma Technology Corporation, Bellows Falls, VT, USA; "red" filter set: 780dxcrr). This made it possible to avoid the inner filter effects related to the high dye concentrations used (10^{-4} M) by focusing the laser near the cuvette window. Residual excitation light was removed using a barrier filter (Chroma Technology; "red": e750sp–2p). The fluorescence was coupled into a 600 µm multimode fibre with an achromatic doublet. The fibre was connected to a compact CCD-based spectrometer (BTC112-E, B&WTek, Newark DE, USA), which measured the two-photon excited emission spectrum. The emission spectra were corrected for the wavelength dependence of the detection efficiency using correction factors established through the measurement of reference compounds having known fluorescence emission spectra. Briefly, the setup allowed for the recording of corrected fluorescence emission spectra under multiphoton excitation at variable excitation power and wavelengths. Further, 2PA cross-sections (σ_2) were determined from the two-photon excited fluorescence (TPEF) cross-sections ($\sigma_2 \cdot \Phi_F$) and the fluorescence emission quantum yield (Φ_F). TPEF cross-sections of 10^{-4} M dichloromethane solutions were measured relative to fluorescein in 0.01 M aqueous NaOH using the well-established method described by Xu and Webb [81] and the appropriate solvent-related refractive index corrections [82]. To check the absence of aggregation, UV–Vis absorption spectra of the dyes were recorded at this concentration in cells of 1 mm pathlength and compared with those obtained with diluted solutions in cells of 1 cm pathlength.

4.5. DFT Computations

DFT and TD-DFT calculations reported in this study were performed using the Gaussian09 [83] program. The geometries of all compounds were optimised without symmetry constraints using the CAM-B3LYP [84] or the MPW1PW91 [57] functionals and the 6-31G* basis set. The solvent effects were taken into account by means of the polarizable continuum model (PCM) [85]. Calculations of the normal modes of vibration were carried out to confirm the true minima character of the optimised geometries. TD-DFT calculations were performed at the same level of theory using the previously optimised geometries. A value of 0.1 was considered for the damping parameter when simulating the electronic spectra (ESI). Swizard [86] was used to plot the simulated spectra, and GausView [87] was used for the MO plots. Subsequently, the 2PA properties were calculated for selected compounds using the SAOP model potential [88,89] (statistical average of orbital model exchange-correlation potential) using the damped cubic response theory module of Jensen et al. [60] implemented in the ADF program package [90], considering the different molecules in the gas phase with the optimised geometries obtained in solution (CH_2Cl_2). The lifetime of the electron-

ically excited states was included in the theory using a damping parameter of 0.0034 au ($\sim$0.1 eV $\sim$ 800 cm^{-1}) value, which was found suitable for 2PA computations [91,92]. The 2PA cross-section σ_2 was obtained from the imaginary part of the third-order hyperpolarizability γ using ad hoc expressions (see ESI) [59]. Cross-section (σ_2) values are usually given in Göppert–Mayer units (1 GM = 10^{-50} $cm^4 \cdot s \cdot photon^{-1}$), so we first evaluated them in atomic units and then multiplied them by $(0.529177 \times 10^{-8}$ cm/a.u.$)^4 \times (2.418884 \times 10^{-17}$ s/a.u.) to obtain values in the conventional units ($cm^4 \cdot s \cdot photon^{-1}$).

5. Conclusions

The two-photon absorption properties of several 2,4,6-triaryl-s-triazines derivatives such as **3-X** (X = NO_2, CN, H, OMe, NMe_2, NPh_2), **4**, and **7-X** (X = H, NPh_2) were studied. After characterising the new members of these families (X = **3-NO_2**, **3-NMe_2**, **4**, **7-H**, and **7-NPh_2**), we uncovered evidence that significant 2PA occurs at the near-IR edge (730–820 nm) for most of them. Similar to what was previously shown for 1,3,5-triarylbenzene or *N*,*N*′,*N*″-triarylisocyanurate analogues, this nonlinear absorption process apparently populates the π-π* charge-transfer excited state(s) at the lowest energy. As confirmed by DFT calculations, the charge transfer occurring during 2PA corresponds to a shift of electron density from the periphery (arms) toward the central ring, except for strongly electron-withdrawing X substituents (X = NO_2 and CN) for which the charge transfer direction reverts. Based on our calculations, compared with **1-X** and **2-X**, the improved 2PA properties of **3-X** derivatives find their origin in the quasi-planar conformation adopted by these molecules in solution and also in the increased polarisation of their π manifold, two features directly resulting from the presence of the central s-triazine unit. The latter favours π-π interactions between peripheral arms and the central core, resulting in a smaller HOMO–LUMO gap for these molecules. We also showed that all **3-X** and **7-X** derivatives featuring neutral to electron-releasing peripheral groups were sufficiently emissive for performing two-photon imaging purposes in solution ($\Phi_F > 0.2$). Actually, in line with extent data for other s-triazines in the literature, they presented larger two-photon brightness than all **1-X**, **2-X**, and **6-X** fluorophores investigated so far. This statement, coupled to the fact that their first 2PA peak is always bathochromically shifted relative to that of their 1,3,5-triarylbenzene or *N*,*N*′,*N*″-triaryl isocyanurate analogues, points to a larger potential for **3-X** derivatives, with **3-NMe_2** and **3-NPh_2** being the most promising molecules in this respect. Provided that such compounds can now be made water-soluble without changing the observed trends, they should give rise to appealing new two-photon dyes for fluorescence bioimaging. Research along these lines is in progress.

Supplementary Materials: The following supporting information can be downloaded at: https://www.mdpi.com/article/10.3390/photochem2020023/s1, Experimental part; NMR, absorption, and emission spectra of **3-X** derivatives; TPEF data for selected **3-X** derivatives; Cartesian coordinates of optimised geometries and selected FMOs for **3-X** and related model derivatives; computed dipole moments and bandgaps; computed 1PA (TD-DFT) and 2PA (-DPZ) spectra; derivation of N_{eff} values.

Author Contributions: Conceptualisation, F.P.; funding acquisition, F.P.; investigation, A.G.B., N.R. and A.A.; methodology, A.G.B. and N.R.; resources, M.B.-D.; supervision, A.B., O.M. and F.P.; writing—original draft preparation, A.G.B. and A.A.; writing—review and editing, A.B., O.M. and F.P. All authors have read and agreed to the published version of the manuscript.

Funding: This project was supported by Région Bretagne (SAD Project *Fotoporf*, N°7205) and ANR (ANR-17-CE07-0033-01 project).

Data Availability Statement: Not applicable.

Acknowledgments: The Region Bretagne (PhD grant for A.G.B.) and ANR (*Isogate* Project) are acknowledged for financial support. We also acknowledge the HPC resources of CINES and of IDRIS under the allocations [2021-x080649] made by GENCI (Grand Equipement National de Calcul Intensif), as well as the SIR platform of ScanMAT at the University of Rennes 1 for technical assistance during the Raman measurements.

Conflicts of Interest: The authors declare no conflict of interest.

Sample Availability: Samples of the compounds are available from the authors.

References and Notes

1. Wolff, J.J.; Wortmann, R. Organic materials for non-linear optics. *J. Prakt. Chem.* **1998**, *340*, 99–111. [CrossRef]
2. Zyss, J.; Ledoux, I. Nonlinear optics in multipolar media: Theory and experiment. *Chem. Rev.* **1994**, *94*, 77–105. [CrossRef]
3. Lee, S.-H.; Park, J.-R.; Jeong, M.-Y.; Kim, H.M.; Li, S.; Song, J.; Ham, S.; Jeon, S.-J.; Cho, B.R. First hyperpolarizability of 1,3,5-Tricyanobenzene Derivatives: Origin of Larger beta Values for the Octupoles than for the Dipoles. *ChemPhysChem* **2006**, *7*, 206–212. [CrossRef] [PubMed]
4. Brunel, J.; Mongin, O.; Jutand, A.; Ledoux, I.; Zyss, J.; Blanchard-Desce, M. Propeller-shaped octupolar molecules derived from triphenylbenzene for nonlinear optics: Synthesis and optical studies. *Chem. Mater.* **2003**, *15*, 4139–4148. [CrossRef]
5. Terenziani, F.; Katan, C.; Badaeva, E.; Tretiak, S.; Blanchard-Desce, M. Enhanced Two-Photon Absorption of Organic Chromophores: Theoretical and Experimental Assessments. *Adv. Mater.* **2008**, *20*, 4641–4678. [CrossRef]
6. He, G.S.; Tan, L.-S.; Zheng, Q.; Prasad, P.N. Multiphoton Absorbing Materials: Molecular Designs, Characterizations, and Applications. *Chem. Rev.* **2008**, *108*, 1245–1330. [CrossRef]
7. Cho, B.R.; Son, K.H.; Lee, S.H.; Song, Y.-S.; Lee, Y.-K.; Jeon, S.-J.; Choi, J.H.; Lee, H.; Cho, M. Two Photon Absorption Properties of 1,3,5-Tricyano-2,4,6-tris(styrl)Benzene Derivatives. *J. Am. Chem. Soc.* **2001**, *123*, 10039–10045. [CrossRef]
8. Lee, W.H.; Lee, S.H.; Kim, J.-A.; Choi, J.H.; Cho, M.; Jeon, S.-J.; Cho, B.R. Two Photon Absorption and Nonlinear Optical Properties of Octupolar Molecules. *J. Am. Chem. Soc.* **2001**, *123*, 10658–10667. [CrossRef]
9. Pawlicki, M.; Collins, H.A.; Denning, R.G.; Anderson, H.L. Two-Photon Absorption and the Design of Two-Photon Dyes. *Angew. Chem. Int. Ed.* **2009**, *48*, 3244–3266. [CrossRef]
10. Argouarch, G.; Veillard, R.; Roisnel, T.; Amar, A.; Boucekkine, A.; Singh, A.; Ledoux, I.; Paul, F. Donor-substituted Triaryl-1,3,5-Triazinane-2,4,6-Triones: Octupolar NLO-phores with a Remarkable Transparency–Nonlinearity Trade-off. *New J. Chem.* **2011**, *35*, 2409–2411. [CrossRef]
11. Argouarch, G.; Veillard, R.; Roisnel, T.; Amar, A.; Meghezzi, H.; Boucekkine, A.; Hugues, V.; Mongin, O.; Blanchard-Desce, M.; Paul, F. Triaryl-1,3,5-Triazinane-2,4,6-Triones (Isocyanurates) Peripherally Functionalized by Donor Groups: Synthesis and Study of their Linear and Nonlinear Optical Properties. *Chem. Eur. J.* **2012**, *18*, 11811–11826. [CrossRef] [PubMed]
12. Streatfield, S.L.; Pradels, C.; Ngo Ndimba, A.; Richy, N.; Amar, A.; Boucekkine, A.; Cifuentes, M.P.; Humphrey, M.G.; Mongin, O.; Paul, F. Electronic Absorption, Emission and Two-Photon Absorption Properties of Some Functional 1,3,5-Triphenylbenzenes. *Chem. Select.* **2017**, *2*, 8080–8085. [CrossRef]
13. Hoffmann, D.K. Model system for a urethane-modified isocyanurate foam. *J. Cell. Plast.* **1984**, *20*, 129–137. [CrossRef]
14. Terenziani, F.; Le Droumaguet, C.; Katan, C.; Mongin, O.; Blanchard-Desce, M. Effect of branching on Two-Photon Absorption in Triphenylbenzene Derivatives. *ChemPhysChem.* **2007**, *8*, 723–734. [CrossRef] [PubMed]
15. Lee, C.-H.; Yammamoto, T. Synthesis of Liquid-Crystalline, Highly Luminescent π-Conjugated 1,3,5-Triazine Derivatives by Palladium-Catalyzed Cross-Coupling Reaction. *Mol. Cryst. Liq. Cryst.* **2002**, *378*, 13–21. [CrossRef]
16. Hu, Q.Y.; Lu, W.X.; Tang, H.D.; Sung, H.H.Y.; Wen, T.B.; Williams, I.D.; Wong, G.K.L.; Lin, Z.; Jia, G. Synthesis and photophysical properties of trimetallic acetylide complexes with a 1,3,5-triazine core. *Organometallics* **2005**, *24*, 3966–3973. [CrossRef]
17. Ranganathan, A.; Heisen, B.C.; Dix, I.; Meyer, F. A triazine-based three directional rigid-rod tecton forms a novel 1D channel structure. *Chem. Commun.* **2007**, *43*, 3637–3639. [CrossRef]
18. Das, P.; Kumar, A.; Chowdhurry, A.; Mukherjee, P.S. Aggregation-Induced Emission and White Luminescence from a Combination of π-Conjugated Donor−Acceptor Organic Luminogens. *ACS Omega* **2018**, *3*, 13757–13771. [CrossRef]
19. Zhang, L.; Zou, L.; Xiao, J.; Zhou, P.; Zhong, C.; Chen, X.; Qin, J.; Mariz, I.F.A.; Maçôas, E. Symmetrical and unsymmetrical multibranched D–π–A molecules based on 1,3,5-triazine unit: Synthesis and photophysical properties. *J. Mater. Chem.* **2012**, *22*, 16781–16790. [CrossRef]
20. Cai, Z.-B.; Chen, L.-J.; Li, S.-L.; Ye, Q.; Tian, Y.-P. Synthesis, electronic structure, linear and nonlinear photophysical properties of novel asymmetric branched compounds. *Dye. Pigm.* **2020**, *175*, 108115. [CrossRef]
21. Cui, Y.Z.; Fang, Q.; Xue, G.; Xu, G.B.; Yin, L.; Yu, W.T. Cooperative enhancement of two-photon absorption of multibranched compounds with vinylenes attaching to the s-triazine core. *Chem. Lett.* **2005**, *34*, 644–645. [CrossRef]
22. Zou, L.; Liu, Z.; Yan, X.; Liu, Y.; Fu, Y.; Liu, J.; Huang, Z.; Chen, X.; Qin, J. Star-Shaped D-π-A Molecules Containing a 2,4,6-Tri(thiophen-2-yl)-1,3,5-triazine Unit: Synthesis and Two-Photon Absorption Properties. *Eur. J. Org. Chem.* **2009**, *2009*, 5587–5593. [CrossRef]
23. Mariz, I.F.A.; Maçôas, E.M.S.; Martinho, J.M.G.; Zou, L.; Zhou, P.; Chen, X.; Qin, J. Molecular architecture effects in two-photon absorption: From octupolar molecules to polymers and hybrid polymer nanoparticles based on 1,3,5-triazine. *J. Mater. Chem. B* **2013**, *1*, 2169–2177. [CrossRef] [PubMed]
24. Liu, S.; Lin, K.S.; Churikov, V.M.; Su, Y.Z.; Lin, J.T.S.; Huang, T.-H.; Hsu, C.C. Two-photon absorption properties of star-shaped molecules containing peripheral diarylthienylamines. *Chem. Phys. Lett.* **2004**, *390*, 433–439. [CrossRef]

25. Zou, L.; Liu, Y.; Ma, N.; Macoas, E.; Martinho, J.M.G.; Pettersson, M.; Chen, X.; Qin, J. Synthesis and photophysical properties of hyperbranched polyfluorenes containing 2,4,6-tris(thiophen-2-yl)-1,3,5-triazine as the core. *Phys. Chem. Chem. Phys.* **2011**, *13*, 8838–8846. [CrossRef]
26. Vidya, V.M.; Chetti, P. A DFT probe on the linear and nonlinear optical characteristics of some star-shaped DI-π-DII-A type acetylene-bridged rigid triazines. *J. Phys. Org. Chem.* **2020**, *33*, e4027.
27. Jiménez-Sánchez, A.; Isunza-Manrique, I.; Ramos-Ortiz, G.; Rodríguez-Romero, J.; Farfán, N.; Santillan, R. Strong Dipolar Effects on an Octupolar Luminiscent Chromophore: Implications on their Linear and Nonlinear Optical Properties. *J. Phys. Chem. A* **2016**, *120*, 4314–4324. [CrossRef]
28. Li, B.; Tong, R.; Zhu, R.; Meng, F.; Tian, H.; Qian, S. The Ultrafast Dynamics and Nonlinear Optical Properties of Tribranched Styryl Derivatives Based on 1,3,5-Triazine. *J. Phys. Chem. B* **2005**, *109*, 10705–10710. [CrossRef]
29. Jiang, Y.; Wang, Y.; Wang, B.; Yang, J.; He, N.; Qian, S.; Hua, J. Synthesis, Two-Photon Absorption and Optical Limiting Properties of Multi-branched Styryl Derivatives Based on 1,3,5-Triazine. *Chem. Asian J.* **2011**, *6*, 157–165. [CrossRef]
30. Gao, Y.; Qu, Y.; Jiang, T.; Zhang, H.; He, N.; Li, B.; Wu, J.; Hua, J. Alkyl-triphenylamine end-capped triazines with AIE and large two-photon absorption cross-sections for bioimaging. *J. Mat. Chem. C* **2014**, *2*, 6353–6361. [CrossRef]
31. Kukhta, N.A.; Simokaitiene, J.; Volyniuk, D.; Ostrauskaite, J.; Grazulevicius, J.V.; Juska, G.; Jankauskas, V. Effect of linking topology on the properties of star-shaped derivativesof triazine and fluorene. *Synth. Met.* **2014**, *195*, 266–275. [CrossRef]
32. Drouet, S.; Merhi, A.; Argouarch, G.; Paul, F.; Mongin, O.; Blanchard-Desce, M.; Paul-Roth, C.O. Synthesis of Luminescent Supramolecular Assemblies from Fluorenyl Porphyrins and Polypyridyl Isocyanurate-based Spacers. *Tetrahedron* **2012**, *68*, 98–105. [CrossRef]
33. Gautier, Y.; Argouarch, G.; Malvolti, F.; Blondeau, B.; Richy, N.; Amar, A.; Boucekkine, A.; Nawara, K.; Chlebowicz, K.; Orzanowska, G.; et al. Triarylisocyanurate-Based Fluorescent Two-Photon Absorbers. *ChemPlusChem* **2020**, *85*, 411–425. [CrossRef] [PubMed]
34. Lee, C.-H.; Yammamoto, T. Synthesis and characterization of a new class of liquid-crystalline, highly luminescent molecules containing a 2,4,6-triphenyl-1,3,5-triazine unit. *Tet. Lett.* **2001**, *42*, 3993–3996. [CrossRef]
35. Iijima, T.; Lee, C.-H.; Fujiwara, Y.; Shimokawa, M.; Suzuki, H.; Yamane, K.; Yamamoto, T. Photoluminescence of 2,4,6-tris[4-(phenylethynyl)phenyl]-1,3,5-triazines dispersed in polymer films. *Opt. Mater.* **2007**, *29*, 1782–1788. [CrossRef]
36. Jiang, Y.; Wang, Y.; Hua, J.; Tang, J.; Li, B.; Qian, S.; Tian, H. Multibranched triarylamine end-capped triazines with aggregation-induced emission and large two-photon absorption cross-sections. *Chem. Commun.* **2010**, *46*, 4689–4691. [CrossRef]
37. Omer, K.M.; Ku, S.-Y.; Chen, Y.-C.; Wong, K.-T.; Bard, A.J. Electrochemical behavior and electrogenerated chemiluminescence of star-shaped D-A compounds with a 1,3,5-triazine core and substituted fluorene arms. *J. Am. Chem. Soc.* **2010**, *132*, 10944–10952. [CrossRef]
38. Aihara, H.; Tanaka, T.; Satou, M.; Yamakawa, T. Synthesis and Electroluminescence of New Organic Emitters Based on a π-Conjugated 1,3,5-Triazine Core. *Trans. Mat. Res. Soc. Jpn.* **2010**, *35*, 675–680. [CrossRef]
39. Jiao, S.; Men, J.; Ao, C.; Huo, J.; Ma, X.; Gao, G. Synthesis and mesophases of C3h-symmetric 2,4,6-tris(2- hydroxyphenyl)-1,3,5-triazine derivatives with intramolecular hydrogen bonding networks. *Tetrahedron Lett.* **2015**, *56*, 5185–5189. [CrossRef]
40. Data, P.; Zassowski, P.; Lapkowski, M.; Grazulevicius, J.V.; Kukhtad, N.A.; Reghu, R.R. Electrochromic behaviour of triazine based ambipolar compounds. *Electrochim. Acta* **2016**, *192*, 283–295. [CrossRef]
41. Idzik, K.R.; Rapta, P.; Cywinski, P.J.; Beckert, R.; Dunsch, L. Synthesis and electrochemical characterization of new optoelectronic materials based on conjugated donor–acceptor system containing oligo-tri(heteroaryl)-1,3,5-triazines. *Electrochim. Acta* **2010**, *55*, 4858–4864. [CrossRef]
42. Furukawa, H.; Go, Y.B.; Ko, N.; Park, Y.K.; Uribe-Romo, F.J.; Kim, J.; O'Keeffe, M.; Yaghi, O.M. Isoreticular Expansion of Metal–Organic Frameworks with Triangular and Square Building Units and the Lowest Calculated Density for Porous Crystals. *Inorg. Chem.* **2011**, *50*, 9147–9152. [CrossRef] [PubMed]
43. Berger, R.; Hauser, J.; Labat, G.; Weber, E.; Hulliger, J. New symmetrically substituted 1,3,5-triazines as host compounds for channel-type inclusion formation. *Cryst. Eng. Comm.* **2012**, *14*, 768–770. [CrossRef]
44. Reimschuessel, H.K.; McDevitt, N.T. Infrared Spectra of Some 1,3,5-Triazine Derivatives. *J. Am. Chem. Soc.* **1960**, *82*, 3756–3762. [CrossRef]
45. Larkin, P.J.; Makowski, M.P.; Colthup, N.B. The form of the normal modes of s-triazine: Infrared and Raman spectral analysis and ab initio force field calculations. *Spectrochim. Acta A* **1999**, *55*, 1011–1020. [CrossRef]
46. In addition to this stretch, a very strong IR- and Raman-active absorption at ca. 1510 ± 5 cm^{-1} was also always observed as an intense mode in IR for all triazine derivatives. Although the C = N stretches in these vibrational modes are certainly admixed with some C-H stretches, we have still labelled them "C = N" in the experimental part.
47. For **3-NPh$_2$**, a correlation between Φ_F and the solvent polarity was stated (e.g., for acetone: Φ_F[400 nm] = 4.3 %, CH2Cl2: Φ_F[406 nm] = 69.1 %, THF: Φ_F[405 nm] = 73 %, Et2O: Φ_F[408 nm] = 87 % and pentane: Φ_F[392 nm] = 95 %). This solvato-fluorochromism was also independently documented in the literature in Das, P. et al. 2018.
48. Stahl, R.; Lambert, C.; Kaiser, C.; Wortmann, R.; Jakober, R. Electrochemistry and photophysics of Donor-Substituted Triarylboranes: Symmetry Breaking in Ground and Excited State. *Chem. Eur. J.* **2006**, *12*, 2358–2370. [CrossRef]

49. Katan, C.; Terenziani, F.; Mongin, O.; Werts, M.H.V.; Porrès, L.; Pons, T.; Mertz, J.; Tretiak, S.; Blanchard-Desce, M. Effects of (Multi)branching of Dipolar Chromophores on Photophysical Properties and Two-Photon Absorption. *J. Phys. Chem. A* **2005**, *109*, 3024–3037. [CrossRef]
50. Bangal, P.R.; Lam, D.M.K.; Peteanu, L.A.; van der Auweraer, M.J. Excited-State localization ina 3-Fold-Symmetric Molecule as Probed by Electroabsorption Spectroscopy. *J. Phys. Chem. B* **2004**, *108*, 16834–16840. [CrossRef]
51. Kim, H.M.; Cho, B.R. Two-photon materials with large two-photon cross sections. Structure-property relationship. *Chem. Commun.* **2009**, *45*, 153–164. [CrossRef]
52. Kuzyk, M.G. Fundamental limits on two-photon absorption cross-sections. *J. Chem. Phys.* **2003**, *119*, 8327–8334. [CrossRef]
53. Amar, A.; Boucekkine, A.; Paul, F.; Mongin, O. DFT study of two-photon absorption of octupolar molecules. *Theo. Chem. Acc.* **2019**, *138*, 1–7. [CrossRef]
54. Kuzyk, M.G. Using fundamental principles to understand and optimize nonlinear-optical materials. *J. Mater. Chem.* **2009**, *19*, 7444–7465. [CrossRef]
55. Webber, A.L.; Yates, J.R.; Zilka, M.; Sturniolo, S.; Uldry, A.-C.; Corlett, E.K.; Pickard, C.J.; Pérez-Torralba, M.; Angeles Garcia, M.; Santa Maria, D.; et al. Weak Intermolecular CH···N Hydrogen Bonding: Determination of 13CH–15N Hydrogen-Bond Mediated J Couplings by Solid-State NMR Spectroscopy and First-Principles Calculations. *J. Phys. Chem. A* **2020**, *124*, 560–572. [CrossRef] [PubMed]
56. Desiraju, G.R. Hydrogen bridges in crystal engeneering: Interactions without border. *Acc. Chem. Res.* **2002**, *35*, 565–573. [CrossRef] [PubMed]
57. Adamo, C.; Barone, V. Exchange functionals with improved long-range behavior and adiabatic connection methods without adjustable parameters: The mPW and mPW1PW models. *J. Chem. Phys.* **1998**, *108*, 664–675. [CrossRef]
58. The CAM-B3LYP computed longest wavelengths are within 2100 cm^{-1} of the experimental data for all derivatives (and below 4000 cm^{-1} for MPW1PW91 functional).
59. Amar, A.; El Kechai, A.; Halet, J.-F.; Paul, F.; Boucekkine, A. Two-photon absorption of dipolar and quadrupolar oligothiophene-cored chromophores derivatives containing terminal dimesitylboryl moieties: A theoretical (DFT) structure-property investigation. *New J. Chem.* **2021**, *45*, 15074–15081. [CrossRef]
60. Hu, Z.; Autschbach, J.; Jensen, L. Simulating Third-Order Nonlinear Optical Properties Using Damped Cubic Response Theory within Time-Dependent Density Functional Theory. *J. Chem. Theory Comput.* **2016**, *12*, 1294–1304. [CrossRef]
61. Strickler, S.J.; Berg, R.A. Relationship between absorption intensity and fluorescence lifetime of molecules. *J. Chem. Phys.* **1962**, *37*, 814–822. [CrossRef]
62. Rabouël, I.; Richy, N.; Amar, A.; Boucekkine, A.; Roisnel, T.; Mongin, O.; Humphrey, M.G.; Paul, F. 1,3,5-Triaryl-1,3,5-Triazinane-2,4,6-Trithiones: Synthesis, Electronic Structure and Linear Optical Properties. *Molecules* **2020**, *25*, 5475. [CrossRef]
63. Considering that these compounds have a quite comparable two-photon brightness, part of this discrepancy could originate from underestimation of the quantum yield of **13-H** in THF (Φ_F = 0.26), since we found Φ_F = 0.78 for **7-H** in THF.
64. Kannan, R.; He, G.S.; Lin, T.-C.; Prasad, P.N.; Vaia, R.A.; Tan, L.-S. Toward highly active two-photon absorbing liquids. Synthesis and characterization of 1,3,5-triazine-based octupolar molecules. *Chem. Mater.* **2004**, *16*, 185–194. [CrossRef]
65. In this respect, the larger Neff numbers presently considered for s-triazines derivatives (see ESI) reflect (at least in part) the beneficial effect of having the peripheral units coplanar with the central core. However, even when the 2PA cross-sections are corrected for these larger numbers of effective electrons (N_{eff}) using the ad hoc figures of merit ($\sigma_2/(N_{eff})^2$), the trend previously observed for σ_2 values is still apparent suggesting that another factor is also influential.
66. Beljonne, D.; Wenseleers, W.; Zojer, E.; Shuai, Z.; Vogel, H.; Pond, S.J.K.; Perry, J.W.; Marder, S.R.; Brédas, J.-L. Role of dimensionality on the two-photon absorption response of conjugated molecules: The case of octupolar compounds. *Adv. Funct. Mater.* **2002**, *12*, 631–641. [CrossRef]
67. For instance, neglecting differences in relaxation energies, an estimate of the excitonic coupling of ca. 0.04 eV (350 cm^{-1}) was found for **3-OMe** from the energy difference (3V) between the first degenerate set of allowed transition (*E* set under strict D_3 symmetry) and the corresponding (forbidden) excitation of *A* symmetry in MPW1PW91. Likewise, a value of ca. 0.04 eV (320 cm^{-1}) was found for this compound using the SAOP functional. Note that during these computational approaches, any vibronic contribution was not considered, Macak, P. et al. 2000 but the latter should also remain weak according to the apparent good match (degeneracy) between twice the wavelength of the 1PA transition and that of the 2PA transition experimentally stated (ESI, Figure S9) Beljonne, D. et al. 2002.
68. Macak, P.; Luo, Y.; Norman, P.; Ågren, H. Electronic and vibronic contributions to two-photon absorption of molecules with multi-branched structures. *J. Chem. Phys.* **2000**, *113*, 7055–7061. [CrossRef]
69. Spangler, C.W. Recent development in the design of organic materials for optical power limiting. *J. Mater. Chem.* **1999**, *9*, 2013–2020. [CrossRef]
70. Wortmann, R.; Glania, C.; Krämer, P.; Matschiner, R.; Wolff, J.J.; Kraft, S.; Treptow, B.; Barbu, E.; Längle, D.; Görlitz, G. Nondipolar Structures with Threefold symmetry for Nonlinear Optics. *Chem. Eur. J.* **1997**, *3*, 1765–1773. [CrossRef]
71. Zhou, H.; Zheng, Z.; Xu, G.; Yu, Z.; Yang, X.; Cheng, L.; Tian, X.; Kong, L.; Wu, J.; Tian, Y. 1, 3, 5-Triazine-cored derivatives dyes containing triphenylamine based two-photon absorption: Synthesis, optical characterization and bioimaging. *Dye. Pigm.* **2012**, *94*, 570–582. [CrossRef]
72. Shriver, D.F.; Drezdzon, M.A. *The Manipulation of Air-Sensitive Compounds*; Wiley: New York, NY, USA, 1986.

73. Gottlieb, H.E.; Kotlyer, V.; Nudelman, A. NMR Chemical Shifts of Common Laboratory Solvents as Trace Impurities. *J. Org. Chem.* **1977**, *62*, 7512–7515. [CrossRef]
74. Fulmer, G.R.; Miller, A.J.M.; Sherden, N.H.; Gottlieb, H.E.; Nudelman, A.; Stoltz, B.M.; Bercaw, J.E.; Goldberg, K.I. NMR Chemical Shifts of Trace Impurities: Common Laboratory Solvents, Organics, and Gases in Deuterated Solvents Relevant to the Organometallic Chemist. *Organometallics* **2010**, *29*, 2176–2179. [CrossRef]
75. Ziessel, R.; Suffert, J.; Youinou, M.-T. General method for the preparation of alkyne-functionalized oligopyryridine building blocks. *J. Org. Chem.* **1996**, *61*, 6535–6546. [CrossRef]
76. Lavastre, O.; Cabioch, S.; Dixneuf, P.H.; Vohlidal, J. Selective and Efficient Access to *Ortho*, *Meta* and *Para* Ring-substituted Phenylacetylene Derivatives R-[CC-C_6H_4]$_x$-Y (Y:H, NO_2, CN, I, NH_2). *Tetrahedron* **1997**, *53*, 7595–7604. [CrossRef]
77. Lim, J.; Albright, T.A.; Martin, B.R.; Miljanić, O.Š. Benzobisoxazole Cruciforms: Heterocyclic Fluorophores with Spatially Separated Frontier Molecular Orbitals. *J. Org. Chem.* **2011**, *76*, 10207–10219. [CrossRef]
78. Malvolti, F.; Rouxel, C.; Triadon, A.; Grelaud, G.; Richy, N.; Mongin, O.; Blanchard-Desce, M.; Toupet, L.; Abdul Razak, F.I.; Stranger, R.; et al. 2,7-Fluorenediyl-bridged Complexes Containing Electroactive "Fe(eta5-C5Me5)(eta2-dppe)C≡C-" Endgroups: Molecular Wires and Remarkable Nonlinear Electrochromes. *Organometallics* **2015**, *34*, 5418–5437. [CrossRef]
79. Demas, N.; Crosby, G.A. Measurement of photoluminescence quantum yields. *J. Phys. Chem.* **1971**, *75*, 991–1024.
80. Eaton, G.R. Reference Materials for Fluorescence Measurement. *Pure Appl. Chem.* **1988**, *60*, 1107–1114. [CrossRef]
81. Xu, C.; Webb, W.W. Measurement of two-photon excitation cross sections of molecular fluorophores with data from 690 to 1050 nm. *J. Opt. Soc. Am. B* **1996**, *13*, 481–491. [CrossRef]
82. Werts, M.H.V.; Nerambourg, N.; Pélégry, D.; Le Grand, Y.; Blanchard-Desce, M. Action cross sections of two-photon excited luminescence of some Eu(III) and Tb(III) complexes. *Photochem. Photobiol. Sci.* **2005**, *4*, 531–538. [CrossRef]
83. Frisch, M.J.; Trucks, G.W.; Schlegel, H.B.; Scuseria, G.E.; Robb, M.A.; Cheeseman, J.R.; Scalmani, G.; Barone, V.; Petersson, G.A.; Nakatsuji, H.; et al. *Gaussian 09*; Revision A.03; Gaussian, Inc.: Wallingford, CT, USA, 2016.
84. Yanai, T.; Tew, D.P.; Handy, N.C. A new hybrid exchange-correlation functional using the Coulomb-attenuating method (CAM-B3LYP). *Chem. Phys. Lett.* **2004**, *393*, 51–57. [CrossRef]
85. Tomasi, J.; Mennucci, B.; Cammi, R. Quantum Mechanical Continuum Solvation Models. *Chem. Rev.* **2005**, *105*, 2999–3093. [CrossRef]
86. Gorelsky, S.I. *SWizard Program, Revision 4.5*; University of Ottawa: Ottawa, ON, Canada, 2013. Available online: http://www.sg-chem.net/ (accessed on 5 February 2022).
87. Dennington, R.; Keith, T.; Millam, J. *GaussView*; Version 5; Semichem Inc.: Shawnee Mission, KS, USA, 2009.
88. Schipper, P.R.T.; Gritsenko, O.V.; van Giesbergen, J.A.; Baerends, E.J. Molecular calculations of excitation energies and (hyper)polarizabilities with a statistical average of orbital model exchange-correlation potentials. *J. Chem. Phys.* **2000**, *112*, 1344–1352. [CrossRef]
89. Jensen, J.F.; van Duijnen, P.T.; Snijders, J.G.J. A discrete solvent reaction field model for calculating frequency-dependent hyperpolarizabilities of molecules in solution. *J. Chem. Phys.* **2003**, *119*, 12998–13005. [CrossRef]
90. *ADF2019*; Vrije Universiteit: Amsterdam, The Netherlands, 2019; Available online: www.scm.com (accessed on 14 May 2022).
91. Jensen, J.F.; Autschbach, J.; Schatz, J. Finite lifetime effects on the polarizability within time-dependent density-functional theory. *J. Chem. Phys.* **2005**, *122*, 224115. [CrossRef]
92. Hu, Z.; Autschbach, J.; Jensen, L. Simulation of resonance hyper-Rayleigh scattering of molecules and metal clusters using a time-dependent density functional theory approach. *J. Chem. Phys.* **2014**, *141*, 124305. [CrossRef] [PubMed]